Bioorganic Chemistry 84 (2019) 276–284

Contents lists available at ScienceDirect

Bioorganic Chemistry

journal homepage: www.elsevier.com/locate/bioorg

# 3D-QSAR assisted identification of FABP4 inhibitors: An effective scaffold hopping analysis/QSAR evaluation

Giuseppe Floresta[a,b,c,*], Agostino Cilibrizzi[c,d], Vincenzo Abbate[d], Ambra Spampinato[a], Chiara Zagni[a], Antonio Rescifina[a,*]

[a] Department of Drug Sciences, University of Catania, V.le A. Doria 6, 95125 Catania, Italy
[b] Department of Chemical Sciences, University of Catania, V.le A. Doria, 95125 Catania, Italy
[c] Institute of Pharmaceutical Science, King's College London, Stamford Street, London SE1 9NH, UK
[d] King's Forensics, School of Population Health & Environmental Sciences, King's College London, Franklin-Wilkins Building, 150 Stamford Street, London SE1 9NH, UK

ARTICLE INFO

*Keywords:*
FABP4 inhibitors
aP2
A-FABP
3D-QSAR
Scaffold-hopping
BMS309403 analogs
Thiazole
Triazole
Forge and Spark software

ABSTRACT

Following on the recent publication of pharmacologically relevant effects, small molecule inhibitors of adipocyte fatty-acid binding protein 4 (FABP4) have attracted high interest. FABP4 is mainly expressed in macrophages and adipose tissue, where it regulates fatty acid storage and lipolysis, being also an important mediator of inflammation. In this regard, FABP4 recently demonstrated an interesting molecular target for the treatment of type 2 diabetes, other metabolic diseases and some type of cancers. In the past years, hundreds of effective FABP4 inhibitors have been synthesized. In this paper, a quantitative structure-activity relationship (QSAR) model has been produced, in order to predict the bioactivity of FABP4 inhibitors. The methodology has been combined with a scaffold-hopping approach, allowing to identify three new molecules that act as effective inhibitors of this protein. These molecules, synthesized and tested for their FABP4 inhibitor activity, showed $IC_{50}$ values between 3.70 and 5.59 μM, with a high level of agreement with the predicted values.

## 1. Introduction

Fatty acids (FAs) are a class of carboxylic acids that carries out different vital functions in the organism [1]. Recently, it was proved that chronically elevated plasma fatty acids lead to specific physiological disorders [2]. For instance, FAs elevated levels are connected with type 2 diabetes [3], obesity [4] and atherosclerosis [5]. Due to the poor solubility in water of FAs, their trafficking requires a cluster of specific carrier proteins, such as albumin, lipocalins and fatty acid-binding proteins (FABPs), that facilitates their transport increasing their water solubility [6]. The adipocyte FABP (A-FABP, aP2 or FABP4) is highly expressed in adipocytes and it is regulated by peroxisome-proliferator-activated receptor-c agonists, as well as by the levels of insulin and fatty acids [7]. Studies in FABP4 knockout mice have shown that FABP4 has a key role in many aspects of the metabolic syndrome [8,9], showing that the lack of this protein partially prevents the advancement of insulin resistance and obesity in mice.

Therefore, pharmacological agents that inhibit FABP4 function can mimic the phenotype of FABP4-deficient mice and small molecules that inhibit FABP4 might be useful candidates for the treatment of metabolic syndromes. FABPs play also an important role in carcinogenesis [10]. Modified FABPs expression were described for prostate, bladder, renal cell carcinoma and other types of cancer cells [11–13], although FABPs biological function in cancer remains mostly unclear [14].

Recently, a variety of effective FABP4 inhibitors have been developed [15], but unfortunately, none of them is currently in the clinical research phases, and only BMS309403 (Fig. 1) has been systematically studied in both *in vitro* and *in vivo* animal models [16–18]. In Table 1 are reported the different classes of FABP4 inhibitors [15], in Fig. 1 and Table 2 some representative examples and their biological evaluations, respectively.

Computer-aided drug design shows a promising and effective tool for the identification of FABP4 inhibitors. Indeed, different structure-based computational approaches have been already performed in the context of FABP4 research, for instance virtual screening studies have been reported with different libraries of compounds, leading to important biological results [27,28]. In line with our recent interest in the development of QSAR models and related applications, in order to identify novel hit compounds, herein we report the development of a 3D-QSAR approach for FABP4 [29–35]. Moreover, the 3D-QSAR model was combined with a scaffold-hopping analysis, allowing the design of new potent molecules able to interact with the binding site and inhibit

* Corresponding authors at: Department of Drug Sciences, University of Catania, V.le A. Doria, 95125 Catania, Italy (G. Floresta, A. Rescifina).
*E-mail addresses:* giuseppe.floresta@unict.it (G. Floresta), arescifina@unict.it (A. Rescifina).

https://doi.org/10.1016/j.bioorg.2018.11.045
Received 4 October 2018; Received in revised form 20 November 2018; Accepted 24 November 2018
Available online 29 November 2018

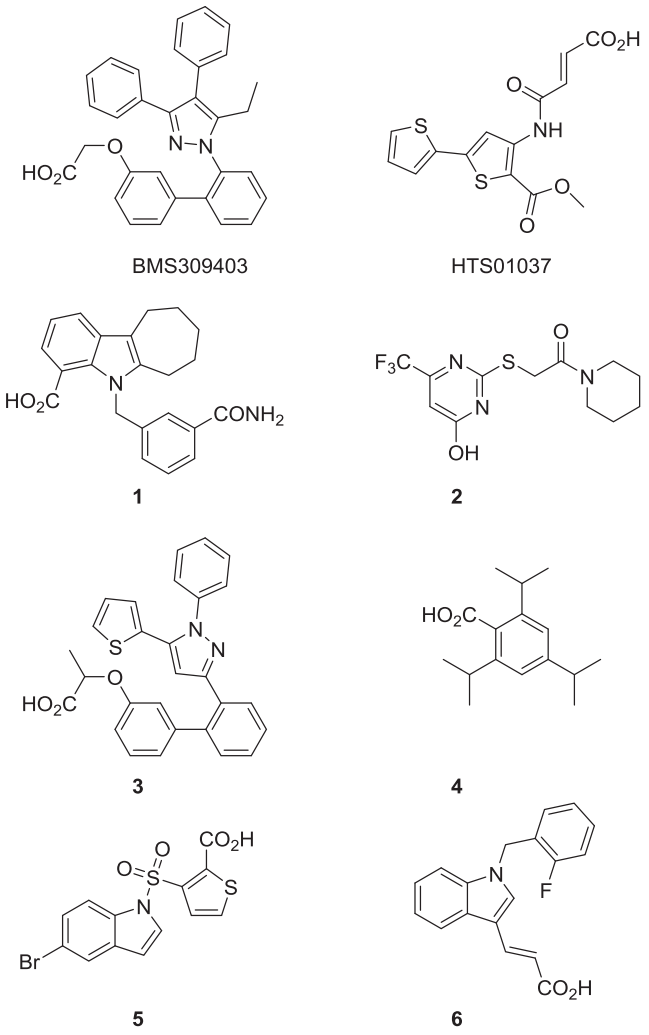


**Fig. 1.** Structures of different FABP4 selective inhibitors.

the FABP4. The 3D-QSAR model for the determination of FABP4 endpoints was developed using the software Forge, while Spark was adopted to produce a scaffold-hopping analysis and generate a virtual library of FABP4 inhibitors. This 3D-QSAR model was used to elucidate SAR data and predict FABP4 endpoints for new molecules. Three of the ligands suggested by the scaffold-hopping analysis were synthesized and tested *in vitro* yielding $IC_{50}$ values between 3.70 and 5.59 μM.

## 2. Results and discussion

### 2.1. Statistical analysis

The regression method used in Forge was PLS (SIMPLS algorithm) [36–40]. As presented in the Data in Brief related article, two different alignment methods were initially tested (*i.e.*, structure-based and ligand-based). The predictive ability of the generated QSAR model was confirmed by several statistical tests. The cross-validation regression coefficient ($q^2$) was calculated based on the PRESS (Prediction error sum of squares) and SSY (Sum of squares of deviation of the experimental values from their mean):

$$q^2 = 1 - \frac{PRESS}{SSY} = 1 - \frac{\sum_{i=1}^{n} (Yexp - Ypred)^2}{\sum_{i=1}^{n} (Yexp - Ymean)^2}$$

*Yexp* = experimental activity of training set compound
*Ypred* = predicted activity of training set compound

**Table 1**
Various chemical classes of FABP4 inhibitors.

| Chemical Classification | Chemical Structure |
|---|---|
| Pyrazole derivatives | 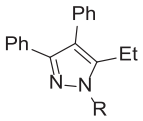 |
| Oxazole derivatives | 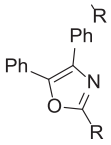 |
| Imidazole derivatives | 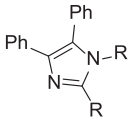 |
| Indole derivatives | 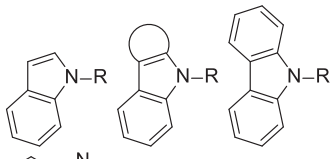 |
| Benzimidazole derivatives | 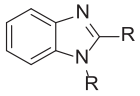 |
| Thiophene and thiazoles derivatives | 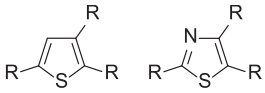 |
| Pyrimidine, bicyclic pyridine and quinoxaline derivatives | 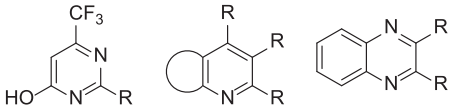 |
| Urea and carbamoyl derivatives | 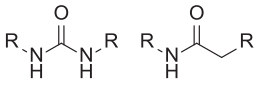 |

**Table 2**
Experimental biological activity of FABP4 inhibitors.

| Compound | $IC_{50}$ or $K_i$ (μM) | Reference |
|---|---|---|
| BMS309403 | 0.71[a] | [19] |
| HTS01037 | 0.67[b] | [20] |
| **1** | 0.45[a] | [21] |
| **2** | 1.00[a] | [22] |
| **3** | 0.001[b] | [23] |
| **4** | 4.00[a] | [24] |
| **5** | 1.30[a] | [25] |
| **6** | 0.033[b] | [26] |

[a] Experimental $IC_{50}$.
[b] Experimental $K_i$.

*Ymean* = mean values of the activity of training set compound

The statistical results of both models are reported in Table 3 and Fig. 2.

As demonstrated above (Fig. 2, Table 3), the ligand-based approach results to be more reliable ($r^2$ = 0.92, $q^2$ = 0.64) than the structure-based alignment, which has an increased noise ($r^2$ = 0.90, $q^2$ = 0.38). At this point, the ligand-based 3D-QSAR align model was further validated with a set of external compounds (*i.e.* test set). Indeed, a more reliable estimation of robustness comes from separate training and test sets. Out of 120 molecules, we randomly choose 96 molecules (covering the whole range of activities of the compounds) as a training set to build the model, while the remaining 24 compounds served as a test set to evaluate the model.

**Table 3**
3D-QSAR model statistics of the different alignment protocols.

| Alignment protocols | Leave-one-out $q^2$ | Training set $r^2$ |
|---|---|---|
| 3D-QSAR Based on Docked Poses (structure based) | 0.38 | 0.90 |
| 3D-QSAR Based on Forge Alignments (ligand based) | 0.64 | 0.92 |

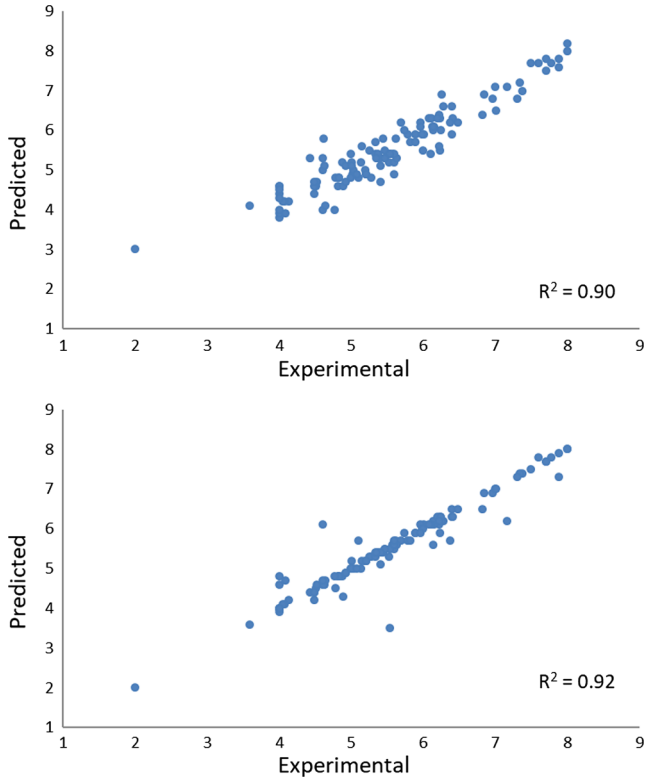


**Fig. 2.** 3D-QSAR model statistics: (up) 3D-QSAR based on docked poses (structure based); (down) 3D-QSAR based on Forge alignments (ligand based).

The statistical reliability of this model was also validated by the determination of the $r^2$test, using the following equation:

$$r^2test = 1 - \frac{\sum_{i=1}^{n} (Ypredtest - Ytest)^2}{\sum_{i=1}^{n} (Ytest - Ymean)^2}$$

*Ypredtest* = predicted activity of test set compound by QSAR equation
*Ytest* = experimental activity of test set compound
*Ymean* = mean values of the activity of training set compound

The results are presented in Figs. 3 and 4. The 11-components model shows both good predictive and descriptive capability as it is shown by the good $r^2$ (0.99) and $q^2$ (0.69) [41] values for the training and the cross-validated training sets. The plot of experimental *vs*. predicted activity for the compounds, in both the training set and the cross-validated training set ($q^2$ = 0.69), shows a reasonable distribution of the values. The plot of experimental *vs*. predicted activity for the compounds in the test set is still reasonably good with only few outliers and a good cross-validated $r^2$ of 0.73.

The graphical interpretation of the model is shown in Fig. 5, where the 3D-QSAR model results are superposed to the structure of the BMS309403. In this model representation, the larger the points are and the stronger is the correlation between the electrostatic/steric fields in that position. This 3D-QSAR model is clearly described by both steric and electrostatic effects and well describes the behavior of the different classes of FABP4 inhibitors inside the binding pocket of FABP4. To

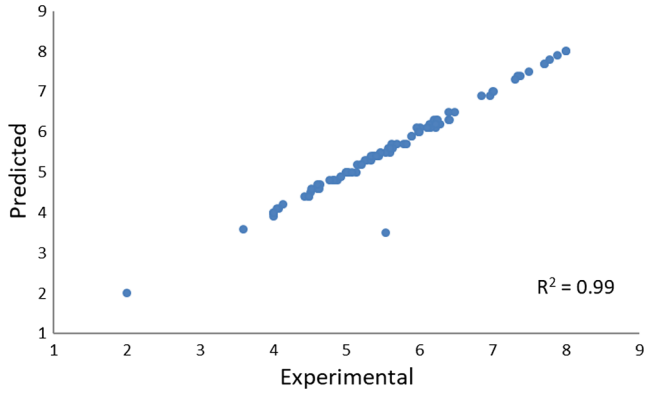


**Fig. 3.** The 11-component 3D-QSAR model – Experimental *vs*. Predicted activity of the compounds in the training set.

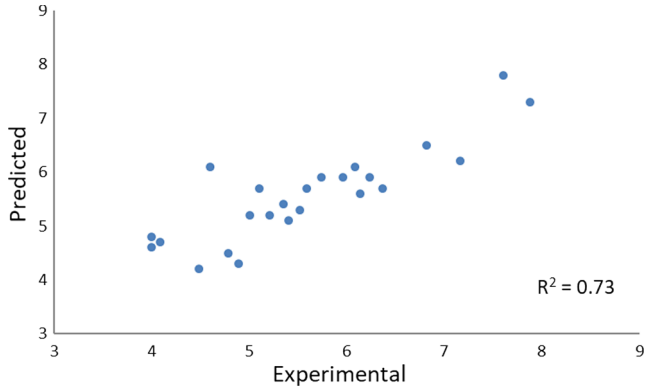


**Fig. 4.** The 11-component 3D-QSAR model – Experimental *vs*. Predicted activity of the compounds in the test set.

reveal the key features of the series under investigation, a structure–-activity relationship (SAR) study was also performed through activity-atlas (AA) visualization software [42]. Fig. 6 illustrates the results of AA calculations, where the AA map is superimposed to BMS309403 lead compound. The different colors on the map highlight electrostatic, hydrophobic and shape features. A more positive electrostatic field increases the receptor-affinity in the red area, whereas in the blue region a more negative electrostatic field increases the affinity. Green and violet areas represent the steric and bulk/hydrophobic interactions. A steric/bulk interaction improves the binding affinity in the green area. On the other hand, in the violet area, a steric/bulk interaction decreases the affinity.

### 2.2. Scaffold-hopping analysis

To design novel hit compounds with FABP4 inhibitory activity, by using the above-reported information from the QSAR model, we decided to use a bioisostere and fragment replacement software tool (*i.e*. Spark; Cresset group) and produce a scaffold hopping analysis to generate a virtual library of FABP4 ligands [43]. As reported in Fig. 7, Different portions of the BMS309403 were studied in the bioisosteric replacement. Once the virtual library was created, the newly designed molecules were scored assuming that if their calculated/aligned fields

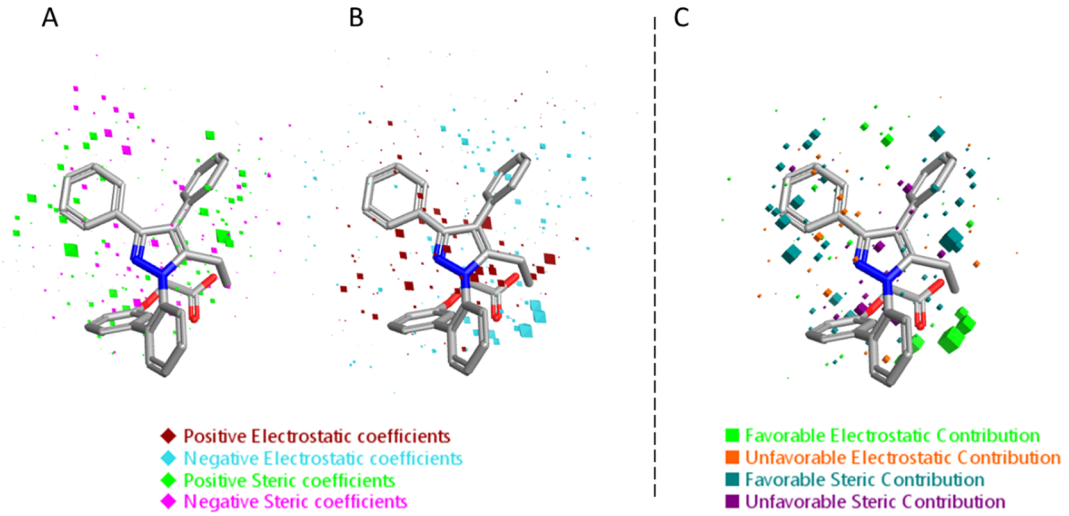


**Fig. 5.** Electrostatic and Steric coefficients for the FABP4 model superposed to the BMS309403. (A) Steric coefficients. (B) Electrostatic coefficients. (C) Contributions to the predicted affinity for BMS309403.

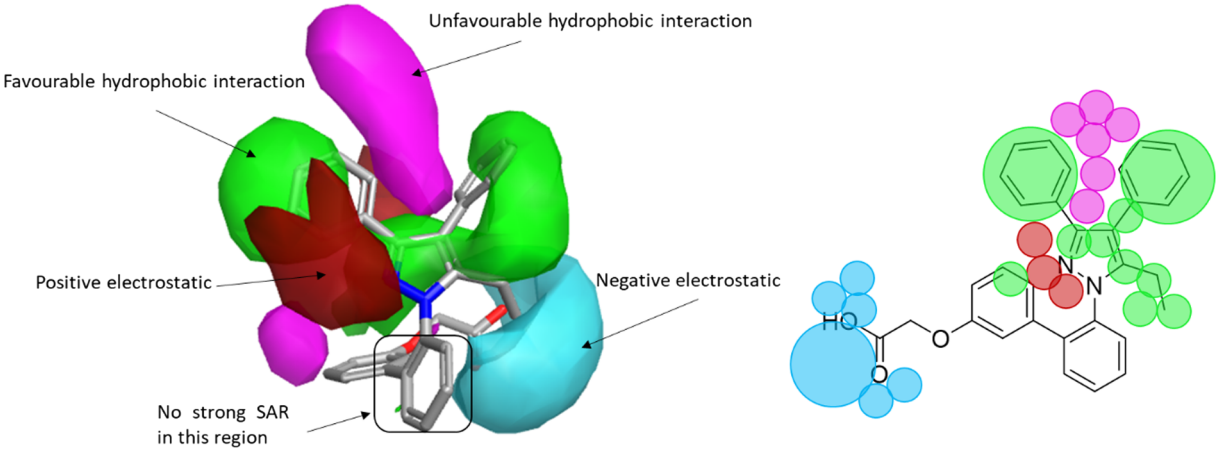


**Fig. 6.** The AA FABP4 model map is superimposed to the BMS309403. Molecular insight of SAR mechanism models, revealing the different lead optimization sites of active compounds. Red color shows positive field region controlling the activity and blue color the negative ones. Green color shows favorable shape/hydrophobic regions and purple color the unfavorable ones.

are highly similar to that of the original compounds present in the 3D-QSAR model, the resulting biological activity would have been comparable [44,45]. The bioisosteric replacement was performed through the same 178,558 fragments for each part, which derive from ChEMBL and Zinc databases [46,47] (see the Data in Brief related article). Five hundred compounds were generated for each substitution producing 3000 hits in total, which were then scored in the 3D-QSAR model.

The first top-scoring compounds (best predicted $pIC_{50}$ values) resulting from the bioisosteric replacement of series 1–6 are reported in Fig. 8, while the full set of compounds are reported as SMILES in the Data in Brief related article. Overall, the results indicate that the bioisosteric replacement and the following 3D-QSAR model evaluation generate compounds with a suitable chemical structure for the inhibition of FABP4.

The results of the scaffold-hopping analysis were used for the design of a novel series of BMS309403-based derivatives. In particular, we focused our attention on the results of the series 3 and 4. In series 3, the most potent compound was predicted as a thiazole derivate of the BMS309403, where the central pyrazole is substituted by a thiazole. In series 4, the most potent predicted compound was the term with a triazole as the aromatic linker, which can be easily introduced through a click chemistry reaction. Using these information, we designed the new series of compounds AST_**1–3** (Fig. 9). The molecules were imported into Forge and aligned/evaluated with the 3D-QSAR model. Interestingly, AST_**1–3** were predicted to have a $pIC_{50}$ of 5.4, 5.9 and 5.6, respectively, and demonstrated an $IC_{50}$ of 3.98, 1.25 and 2.51 μM. To prove the effective predicting capabilities of our model, we decide to set up a synthetic route that affords AST_**1–3**.

### 2.3. Synthesis

The synthesis (Scheme 1) starts from commercially available aldehydes (*i.e.* benzaldehyde, naphthaldehyde, and 4-chloro benzaldehyde) and the Grignard reagent generated *in situ* by benzyl bromide and magnesium. The alcohol **10** was firstly oxidized with PCC (Pyridinium chlorochromate) to give compounds **11** and then monohalogenated, at the *α*-position, with bromine under acidic conditions (compounds **12**). The 2-aminobenzene-1-carbothioamide **14** was generated from the respective amide **13** and the Lawesson's reagent. Subsequently, the thioamide was reacted with intermediate **12** to give the thiazole derivatives **15**. The butynoic acid **17** was obtained by oxidation of 3-butyn-1-ol **16**. Lastly, the treatment of **15** with *t*-BuONO (*tert*-Butyl nitrite) and azidotrimethylsilane afforded the azide intermediate and the final analogs were assembled by using **17** *via* azide-alkyne Huisgen cycloaddition (*i.e.* copper (I) catalyzed variant, where organic azides and terminal alkynes are united to afford 1,4-regioisomers of 1,2,3-triazoles as single products).

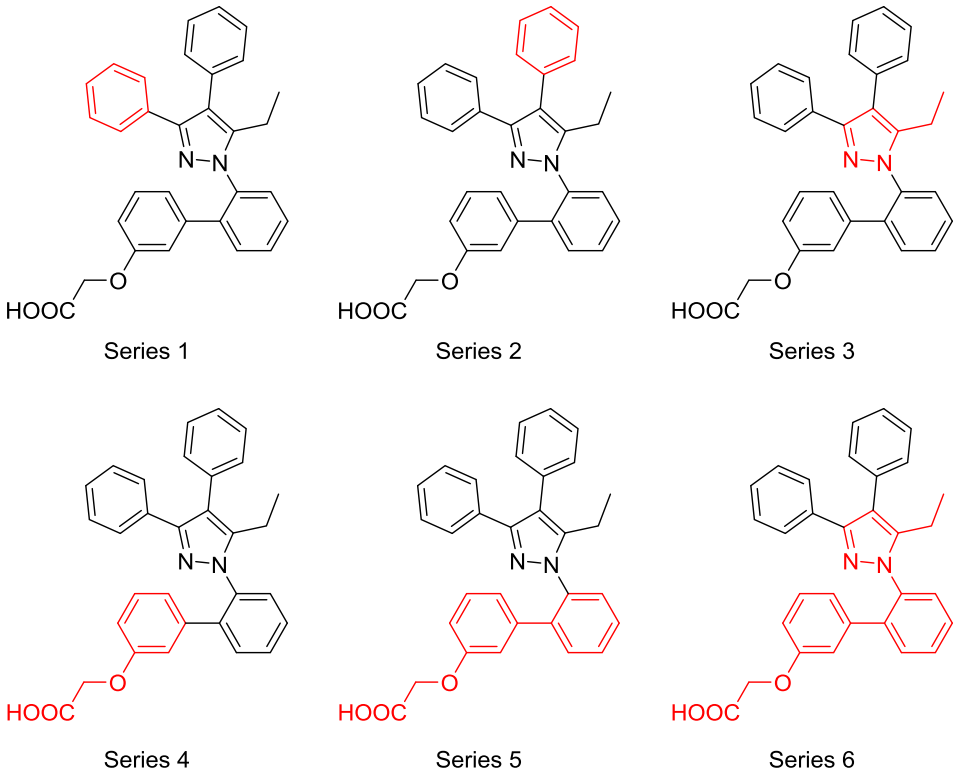


**Fig. 7.** Bioisosteric replacement of the lead compound BMS309403.

### 2.4. FABP4 inhibition evaluation

FABP4 inhibitory activity was determined with a commercially available screening assay kit, by measuring the decreasing in fluorescence of a detection reagent (which is supplied in the kit) when displaced by an inhibitor of FABP4. Specifically, the detection reagent exhibits increased fluorescence when bound to FABP4. Binding of the detection reagent is monitored by exciting at 370 nm and measuring the emission at 470 nm. Therefore, any powerful inhibitor of the protein, which binds to the same binding pocket, can displace the detection reagent, thereby reducing the fluorescence read-out. Inhibition activity data are expressed as $IC_{50}$ (μM) and results obtained with AST_**1–3** are

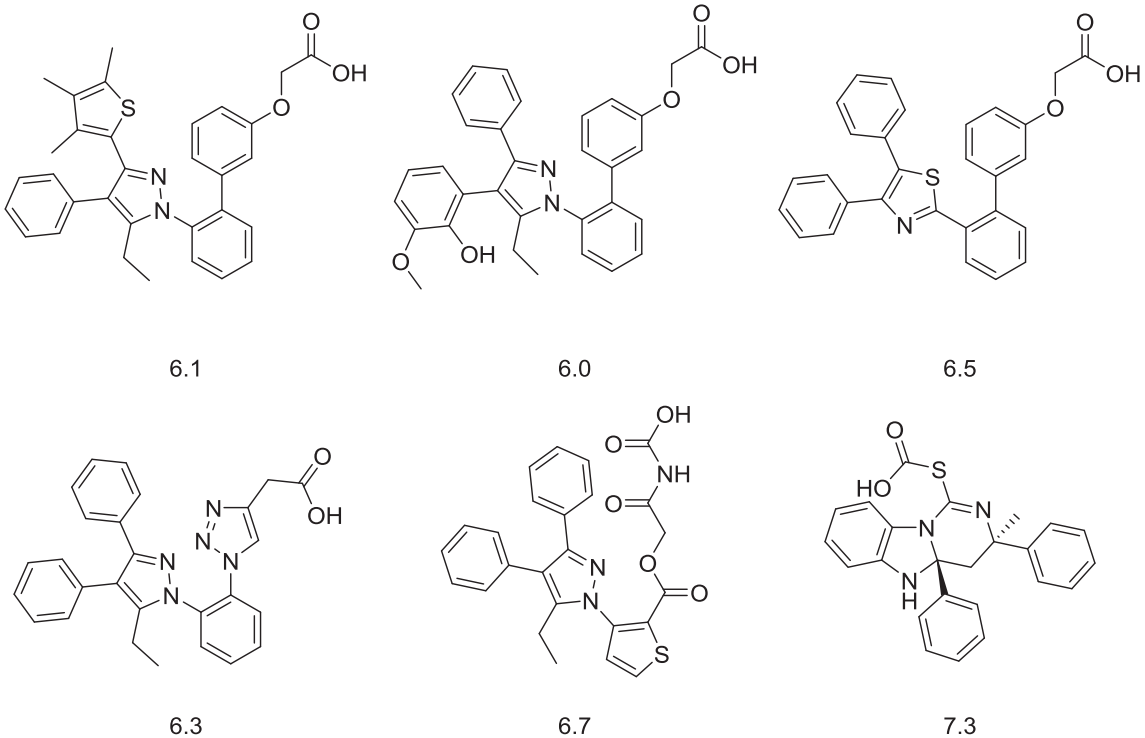


**Fig. 8.** First top-scored compounds derived from series 1–6, with regards to FABP4 predicted $pIC_{50}$.

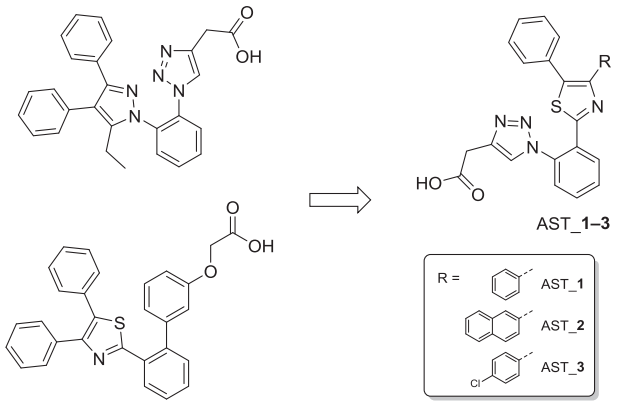


**Fig. 9.** Structures of AST_**1**–**3**.

reported in Table 4. Arachidonic acid, a known powerful ligand of FABP4, was used as a positive control and revealed an $IC_{50}$ of 3.06 μM. Our set of compounds, AST_**1**–**3**, showed $IC_{50}$ values of 5.59, 3.70, and 4.31, respectively.

## 3. Conclusion

FABP4 provides an attractive therapeutic and diagnostic target for a variety of diseases as demonstrated in a variety of animal models [48–51]. FABP4 inhibitors could also be effective for the treatment of cancer patients *via* the inhibition or reduction of early-stage tumors and metastasis. Similarly, they show effective as biomarkers for the diagnosis of different types of cancers [52–58]. In addition, FABP inhibitors could also be used for the treatment of neurological disorders [59–62]. In this study, a 3D-QSAR model for known FABP4 inhibitors was produced and used to study a large library of molecules as possible inhibitors of FABP4, by means of scaffold-hopping analysis. The efficient predictive capabilities of the QSAR model was also proved through the synthesis of three new compounds as FABP4 inhibitors, using the information obtained from the QSAR equation. FABP4 binding affinities of the newly designed compounds (AST_**1**–**3**) were measured by means of an established displacement assay, showing that they are FABP4 inhibitors in the low micromolar range (*i.e.* $IC_{50}$ values between 3.70 and 5.59 μM). Moreover, a large number of different molecules were also theorized to be as effective as the three synthesized and can be a useful starting point for the design of others FABP4 inhibitors. Our results widely demonstrate that simple modifications performed on

**Table 4**
Measured $IC_{50}$ values for Arachidonic acid and AST_**1**–**3** in FABP4.

| Compounds | $IC_{50}$ (μM) |
|---|---|
| Arachidonic acid | 3.06 ± 0.22 |
| AST_**1** | 5.59 ± 0.79 |
| AST_**2** | 3.70 ± 0.34 |
| AST_**3** | 4.31 ± 0.67 |

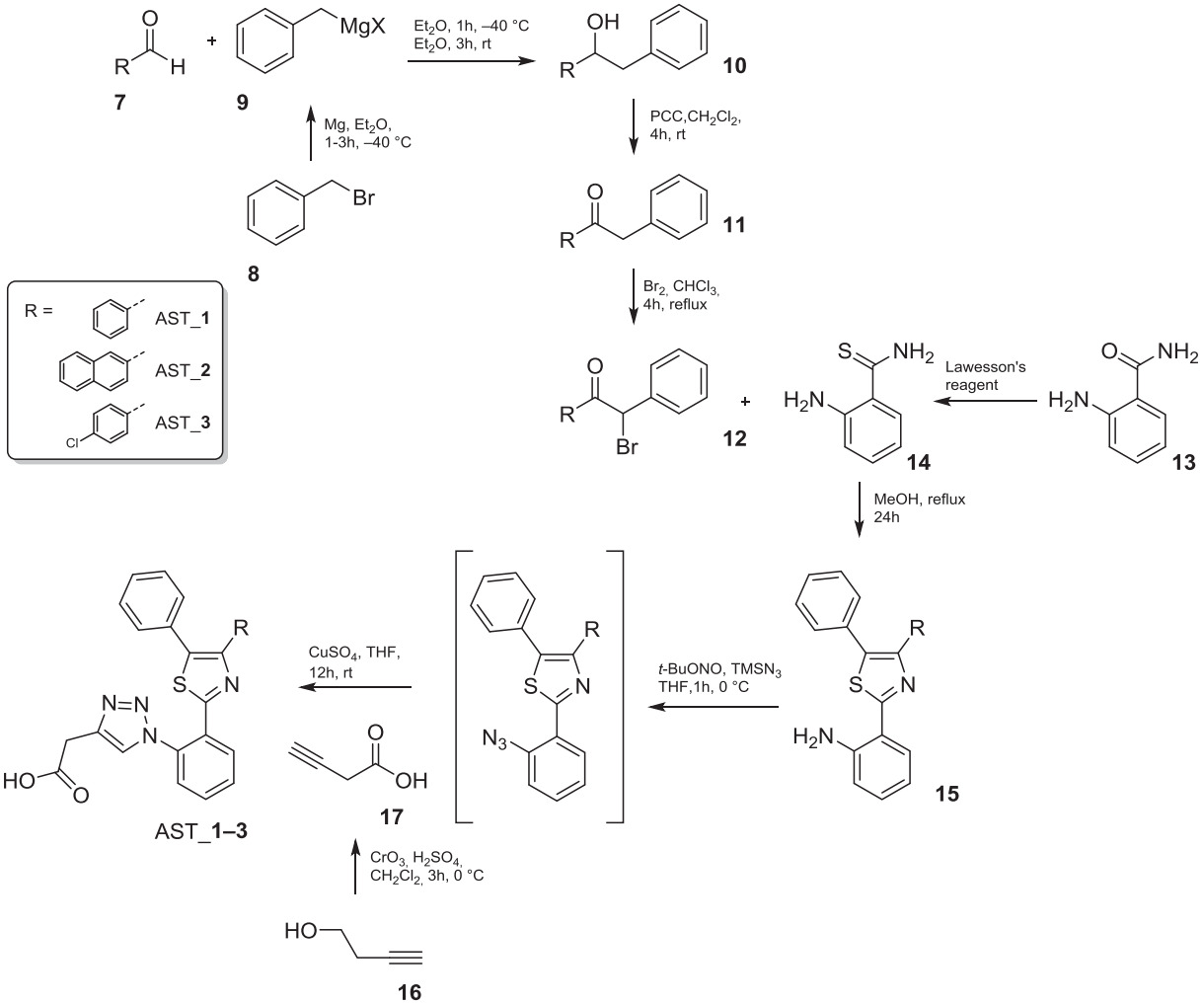


**Scheme 1.** Synthetic scheme for the molecules AST_**1**–**3**.

different sites of the gold standard BMS309403 can retain or even improve FABP4 inhibitory activity of the analogs. These findings, of course, should be validated experimentally but are considered a reasonable starting point for the researchers in the field. Surely, these findings will lead our future research in the field of the development of FABP4 inhibitors. Considering this transporter as a very promising target, the ultimate goal is to finally bring optimized molecules into clinical research phase.

## 4. Experimental section

### 4.1. Molecular modeling and biological data

The 120 structures used to build and evaluate the 3D-QSAR model were chosen among the structures previously published [19,21,22,24,25,63,64]. All molecules possess an excellent selectivity toward the FABP4 and the range of activities is broad enough to be able to build an efficient model. The 2D chemical structures were built by Marvin Sketch, and all structures were subjected to molecular mechanics energy minimization using the MMFF94 force field present in the same software [65]. Once obtained the 3D structures of all compounds the geometry was also optimized at the semi-empirical level of theory using the PM3 Hamiltonian [66], as implemented in MOPAC 2016 package [67]. The protonation states of the molecules were calculated assuming a pH of 7.0. Forge 10.4.2 (Cresset BioMolecular Discovery Ltd., https://www.cresset-group.com/) was used for the building of the 3D-QSAR model. Spark 10.4.0 was used for the scaffold-hopping analysis (Cresset BioMolecular Discovery Ltd., https://www.cresset-group.com/). Forge's parameters used for conformation hunt/alignment and to build/validate the QSAR model are reported in the Data in Brief related article.

### 4.2. Chemistry

All chemicals were purchased from Merk, Sigma Aldrich, and Acros Organics and were reagent grade or better. Solvents were purchased from Fisher Scientific, Sigma Aldrich, and VWR. Silica gel for column chromatography was purchased from Merck. Samples were dried in a vacuum oven (Gallenkamp, rated to ≤250 °C) connected to a vacuum pump (BOC-Edwards.). Pre-coated aluminum sheets (silica gel 60 F254, Merck) were used for thin-layer chromatography (TLC) and spots were visualized under UV light. $^{1}$H NMR and $^{13}$C NMR spectra were recorded on Varian UNITY Inova spectrometer using $CDCl_3$ or DMSO-$d_6$ as a solvent and tetramethylsilane (TMS) as an internal standard, at 200 or 500 MHz for $^{1}$H NMR and 125 MHz for $^{13}$C NMR. $^{13}$C spectra were $^{1}$H decoupled and multiplicities were determined by the APT pulse sequence. Chemical shift ($\delta$) values are given in ppm. All of the NMR experiments were analyzed using the General NMR Analysis Toolbox (GNAT) [68]. Mass spectra were run at King's College London (UK) on a Thermofisher LCQ DECA XP ion trap mass spectrometer or a Waters - Micromass ZQ - Single quadrupole mass spectrometer. HPLC analyses were performed on Agilent 1100 series HPLC with quadrupole pump, vacuum degasser, variable wavelength detector (set to 254 or 281 nm), using a gradient water/acetonitrile as reported in the supporting information. Elemental analyses for C, H, N, and S were performed on a Carlo Erba Elemental Analyzer Mod. 1108 apparatus.

#### 4.2.1. General procedure for the synthesis of alcohols *10*

A solution of benzyl bromide **8** (0.02 mol) in $Et_2O$ (50 mL) was dropwise added to a stirred suspension of Mg (0.025 mol) over a period of 2 h at room temperature. The mixture was stirred for 3 additional hours at room temperature to produce benzyl Grignard **9** and cooled to −40 °C. A solution of aldehyde **7** (0.01 mol) in $Et_2O$ (50 mL) was added over a period of 1 h. The mixture was stirred for 2 h at −40 °C, gradually brought to room temperature and stirred for 3 h more. After addition of saturated aqueous $NH_4Cl$ (10 mL), the mixture was extracted with EtOAc. The combined organic extracts were washed with water, brine and dried over $Na_2SO_4$. Solvent removal under reduced pressure and column chromatography of the residue (silica gel, 93/7, cyclohexane/EtOAc) afforded the pure alcohol **10**. Yields 92–99%.

#### 4.2.2. General procedure for the synthesis of ketones *11*

A solution of **10** (8.0 mmol) was added to a stirred suspension of pyridinium chlorochromate (12 mmol) in $CH_2Cl_2$ (60 mL). The mixture was stirred at room temperature for nearly 3 h until the disappearance of the starting material (monitored by TLC), diluted with diethyl ether (50 mL) and filtered through a column of celite. Solvent removal of the filtrate under reduced pressure and column chromatography of the residue (silica gel, 95/5, cyclohexane/EtOAc) afforded pure **11**. Yields 95–99%.

#### 4.2.3. General procedure for the synthesis of α-bromoketone *12*

Bromine (3.8 mmol) was added dropwise to a solution of **11** (2.5 mmol) in freshly distilled $CHCl_3$ (10 mL). The mixture was heated under reflux until conversion was complete (monitored by TLC). After cooling, the solvent was evaporated under reduced pressure to provide a residue that was purified *via* column chromatography (silica gel, cyclohexane) to yield pure α-bromoketone **12**. Yields 70–85%.

#### 4.2.4. General procedure for the synthesis of 2-Aminothiobenzamide *14*

Lawesson's reagent (8.0 mmol) was added to a solution of **13** (14.7 mmol) in THF (75 mL). The mixture was stirred under $N_2$ at room temperature for 24 h. The solvent was evaporated, and the residue partitioned between EtOAc (50 mL), and 1 N HCl (30 mL). Aqueous sat. $NaHCO_3$ was added to the aqueous layer until pH = 8–9. This basic solution was extracted with EtOAc (30 mL). The combined organic layers were dried ($Na_2SO_4$) and filtered. The solvent was evaporated and the resulting solid residue was recrystallized from toluene to afford pure **14** as a yellow solid; yield 72%.

#### 4.2.5. General procedure for the synthesis of thiazole *15*

The 2-aminothiobenzamide **14** (1.5 mmol) was added to a solution of α-bromoketone **12** (1.0 mmol) in methanol. The mixture was refluxed overnight. After cooling, the solvent was evaporated under reduced pressure to provide a residue that was purified by column chromatography (silica gel, 99/1, cyclohexane/EtOAc) to yield pure thiazoles **15. 15_1**: yield 75%, yellow solid, m.p.: 168–170 °C. $^{1}$H NMR (200 MHz, Chloroform-*d*) $\delta$ 6.22 (bs, 2H), 6.58 – 6.88 (m, 2H), 7.04–7.47 (m, 9H), 7.57 (m, 3H). $^{13}$C NMR (50 MHz, chloroform-*d*) $\delta$ 113.63, 116.77, 116.82, 127.60, 127.68, 127.92, 128.16, 128.55, 128.63, 128.87, 129.58, 129.83, 130.59, 145.64, 149.16, 166.96. **15_2**: yield 76%, yellow solid, m.p.: 178–180 °C. $^{1}$H NMR (200 MHz, chloroform-*d*) $\delta$ 6.42–6.85 (m, 2H), 7.17–7.54 (m, 9H), 7.54–7.89 (m, 6H), 7.99–8.22 (m, 1H), 8.68 (s, 1H). $^{13}$C NMR (50 MHz, chloroform-*d*) $\delta$ 110.92, 115.13, 126.18, 126.27, 126.89, 127.69, 127.79, 128.19, 128.34, 128.78, 129.26, 129.72, 130.87, 131.32, 131.94, 132.56, 132.86, 133.37, 147.61, 148.92.

**15_3**: yield 81%, yellow solid, m.p.: 172–173 °C.

#### 4.2.6. General procedure for the synthesis of 3-butynoic acid *17*

A solution of 21 g (0.3 mol) of 3-butyn-1-ol **16** in acetone (300 mL) was added dropwise to a stirred solution of chromium trioxide (60 g, 0.6 mol) in 750 mL of 10 N $H_2SO_4$ at 0 °C. The reaction mixture was allowed to warm to room temperature and the stirring was continued for 1.5 h. The liquid was decanted into a mixture of EtOAc and $H_2O$. The aqueous layer was extracted five times with EtOAc. The extracts were combined, washed twice with saturated NaCl solution, dried ($Na_2SO_4$) and evaporated. The resulting solid residue was recrystallized from hexane to afford pure **17** as a white solid, yield 93%.

#### 4.2.7. General procedure for the synthesis of final compounds AST_*1–3*

The suitable thiazole **15** (0.54 mmol) was dissolved in THF (2 mL) in

a 25 mL round-bottomed flask and cooled to 0 °C in an ice-bath. *t*-BuONO (0.81 mmol) and $TMSN_3$ (0.65 mmol) were sequentially added to this mixture under stirring. The resulting solution was reacted at room temperature for 2 h. 3-Butinoic acid **17** (0.54 mmol), an aq. solution (0.2 mL) of $CuSO_4$ (0.027 mmol), sodium ascorbate (0.108 mmol) were then added and the reaction was stirred overnight at room temperature. The crude mixture was concentrated under vacuum and the product was then precipitated by addition of water to give the final compounds AST_**1–3**. AST_**1**: white solid, m.p.: 238–240 °C. $^1$H NMR (500 MHz, DMSO-$d_6$) $\delta$ 3.62 (s, 2H), 7.11–7.47 (m, 10H), 7.56 (d, $J$ = 7.5 Hz, 1H), 7.73 (m, 2H), 8.08–8.47 (m, 2H). Anal. Calcd. for $C_{25}H_{18}N_4O_2S$: C, 68.48; H, 4.14; N, 12.78; S, 7.31; found C, 68.11; H, 4.10; N, 12.89; S, 7.22. AST_**2**: white solid, m.p.: 241–243 °C. $^1$H NMR (500 MHz, DMSO-$d_6$) $\delta$ 3.57 (s, 2H), 7.28 (d, $J$ = 7.9 Hz, 2H), 7.36 (m, 3H), 7.43–7.52 (m, 2H), 7.55 (d, $J$ = 7.9 Hz, 1H), 7.64–7.74 (m, 1H), 7.74–7.83 (m, 3H), 7.83–7.91 (m, 1H), 7.95 (s, 1H), 8.26 (d, $J$ = 6.7 Hz, 2H). Anal. Calcd. for $C_{29}H_{20}N_4O_2S$: C, 71.29; H, 4.13; N, 11.47; S, 6.56; found C, 71.54; H, 4.18; N, 11.38; S, 6.33. AST_**3**: white solid, m.p.: 241–242 °C. $^1$H NMR (500 MHz, chloroform-*d*) $\delta$ 3.98 (s, 2H), 7.13 (t, $J$ = 7.8 Hz, 1H), 7.17–7.24 (m, 2H), 7.25–7.37 (m, 5H), 7.44 (t, $J$ = 1.9 Hz, 1H), 7.50 (dd, $J$ = 7.8, 1.3 Hz, 1H), 7.59 (td, $J$ = 7.7, 1.5 Hz, 1H), 7.66 (td, $J$ = 7.7, 1.5 Hz, 1H), 7.89 (s, 1H), 8.15 (dd, $J$ = 7.7, 1.5 Hz, 1H). $^{13}$C NMR (50 MHz, chloroform-*d*) $\delta$ 29.68, 126.94, 127.93, 128.11, 128.72, 128.86, 128.96, 129.35, 129.53, 130.35, 130.70, 134.07, 136.05, 160.12. Anal. Calcd. for $C_{25}H_{17}ClN_4O_2S$: C, 63.49; H, 3.62; N, 11.85; S, 6.78; found C, 63.34; H, 3.61; N, 11.92; S, 6.72.

### 4.3. FABP inhibitory activity assays

To analyze the inhibitory activity of FABP4 ligands, a displacement assay was utilized as described by the Cayman's instruction, FABP4 Inhibitor/Ligand Screening Assay Kit, Item 10010231. The samples of compounds AST_**1–3** for activity determination were prepared as a stock solution (1 mM) in DMSO. On the day of activity assay, the compounds were all diluted in phosphate buffer solution (PBS, pH 7.4) to different concentrations (50, 25, 12.5, 6.25, 3.12, 1.56 and 0.15 μM). Appropriate concentrations of DMSO in PBS was used as control. The detection reagent (FABP Assay Detection Reagent, Item 10010376) was used as provided by the Cayman's kit. The diluted Detection Reagent probe was mixed with FABP4 protein present in the kit and incubated for 10 min at room temperature. Compounds were then added and equilibrated for another 10 min. Lastly, the fluorescence signal was recorded at 470 nm (*i.e.* emission, with the excitation fixed at 370 nm) with a CytoFluor® Series 4000 Fluorescence Multi-Well Plate Reader. The plotted displacement curves for Arachidonic acid (positive control) and AST_**1–3** are reported in the supporting information.

## Acknowledgments

Free academic licenses from Cresset and ChemAxon for their suites of programs are gratefully acknowledged.

## Appendix A. Supplementary material

Supplementary data to this article can be found online at https://doi.org/10.1016/j.bioorg.2018.11.045.

## References

[1] U.N. Das, Essential Fatty acids - a review, Curr. Pharm. Biotechnol. 7 (2006) 467–482.
[2] G. Boden, Free fatty acids (FFA), a link between obesity and insulin resistance, Front. Biosci. 3 (1998) 169–175.
[3] R.A. DeFronzo, Dysfunctional fat cells, lipotoxicity and type 2 diabetes, Int. J. Clin. Pract. Suppl. (2004) 9–21.
[4] S.G. Sheth, F.D. Gordon, S. Chopra, Nonalcoholic steatohepatitis, Ann. Intern. Med. 126 (1997) 137–145.
[5] G. Boden, Obesity and free fatty acids, Endocrinol. Metab. Clin. North Am. 37 (2008) 635–646 viii-ix.
[6] J. Storch, A.E. Thumser, The fatty acid transport function of fatty acid-binding proteins, Biochim. Biophys. Acta 1486 (2000) 28–44.
[7] M.I. Queipo-Ortuno, X. Escote, V. Ceperuelo-Mallafre, L. Garrido-Sanchez, M. Miranda, M. Clemente-Postigo, R. Perez-Perez, B. Peral, F. Cardona, J.M. Fernandez-Real, F.J. Tinahones, J. Vendrell, FABP4 dynamics in obesity: discrepancies in adipose tissue and liver expression regarding circulating plasma levels, PLoS One 7 (2012) e48605.
[8] B.R. Thompson, A.M. Mazurkiewicz-Munoz, J. Suttles, C. Carter-Su, D.A. Bernlohr, Interaction of Adipocyte Fatty Acid-binding Protein (AFABP) and JAK2 AFABP/aP2 AS A REGULATOR OF JAK2 SIGNALING, J. Biol. Chem. 284 (2009) 13473–13480.
[9] A. Adida, F. Spener, Adipocyte-type fatty acid-binding protein as inter-compartmental shuttle for peroxisome proliferator activated receptor gamma agonists in cultured cell, Bba-Mol. Cell Biol. L 1761 (2006) 172–181.
[10] K.M. Nieman, H.A. Kenny, C.V. Penicka, A. Ladanyi, R. Buell-Gutbrod, M.R. Zillhardt, I.L. Romero, M.S. Carey, G.B. Mills, G.S. Hotamisligil, S.D. Yamada, M.E. Peter, K. Gwin, E. Lengyel, Adipocytes promote ovarian cancer metastasis and provide energy for rapid tumor growth, Nat. Med. 17 (2011) 1498–1503.
[11] A. Tolle, S. Suhail, M. Jung, K. Jung, C. Stephan, Fatty acid binding proteins (FABPs) in prostate, bladder and kidney cancer cell lines and the use of IL-FABP as survival predictor in patients with renal cell carcinoma, BMC Cancer 11 (2011) 302.
[12] H. Uehara, T. Takahashi, M. Oha, H. Ogawa, K. Izumi, Exogenous fatty acid binding protein 4 promotes human prostate cancer cell progression, Int. J. Cancer 135 (2014) 2558–2568.
[13] A. Yang, H. Zhang, Y. Sun, Y. Wang, X. Yang, X. Yang, H. Zhang, W. Guo, G. Zhu, J. Tian, Y. Jia, Y. Jiang, Modulation of FABP4 hypomethylation by DNMT1 and its inverse interaction with miR-148a/152 in the placenta of preeclamptic rats and HTR-8 cells, Placenta 46 (2016) 49–62.
[14] D. Lee, K. Wada, Y. Taniguchi, H. Al-Shareef, T. Masuda, Y. Usami, T. Aikawa, M. Okura, Y. Kamisaki, M. Kogo, Expression of fatty acid binding protein 4 is involved in the cell growth of oral squamous cell carcinoma, Oncol. Rep. 31 (2014) 1116–1120.
[15] G. Floresta, V. Pistara, E. Amata, M. Dichiara, A. Marrazzo, O. Prezzavento, A. Rescifina, Adipocyte fatty acid binding protein 4 (FABP4) inhibitors. A comprehensive systematic review, Eur. J. Med. Chem. 138 (2017) 854–873.
[16] A. Bosquet, J. Girona, S. Guaita-Esteruelas, M. Heras, P. Saavedra-Garcia, N. Martinez-Micaelo, L. Masana, R. Rodriguez-Calvo, FABP4 inhibitor BMS309403 decreases saturated-fatty-acid-induced endoplasmic reticulum stress-associated inflammation in skeletal muscle by reducing p38 MAPK activation, Biochim. Biophys. Acta Mol Cell Biol. Lipids 2018 (1863) 604–613.
[17] C. Look, I. Morano, M. Ehrhart-Bornstein, S.R. Bornstein, V. Lamounier-Zepter, BMS309403 directly suppresses cardiac contractile function, Naunyn Schmiedebergs Arch. Pharmacol. 384 (2011) 255–263.
[18] M.Y. Lee, H. Li, Y. Xiao, Z. Zhou, A. Xu, P.M. Vanhoutte, Chronic administration of BMS309403 improves endothelial function in apolipoprotein E-deficient mice and in cultured human endothelial cells, Br. J. Pharmacol. 162 (2011) 1564–1576.
[19] T. Okada, M. Hiromura, M. Otsuka, S. Enomoto, H. Miyachi, Synthesis of BMS-309403-related compounds, including [(1)(4)C]BMS-309403, a radioligand for adipocyte fatty acid binding protein, Chem. Pharm. Bull. (Tokyo) 60 (2012) 164–168.
[20] A.V. Hertzel, K. Hellberg, J.M. Reynolds, A.C. Kruse, B.E. Juhlmann, A.J. Smith, M.A. Sanders, D.H. Ohlendorf, J. Suttles, D.A. Bernlohr, Identification and characterization of a small molecule inhibitor of fatty acid binding proteins, J. Med. Chem. 52 (2009) 6024–6031.
[21] T. Barf, F. Lehmann, K. Hammer, S. Haile, E. Axen, C. Medina, J. Uppenberg, S. Svensson, L. Rondahl, T. Lundback, N-Benzyl-indolo carboxylic acids: design and synthesis of potent and selective adipocyte fatty-acid binding protein (A-FABP) inhibitors, Bioorg. Med. Chem. Lett. 19 (2009) 1745–1748.
[22] R. Ringom, E. Axen, J. Uppenberg, T. Lundback, L. Rondahl, T. Barf, Substituted benzylamino-6-(trifluoromethyl)pyrimidin-4(1H)-ones: a novel class of selective human A-FABP inhibitors, Bioorg. Med. Chem. Lett. 14 (2004) 4449–4452.
[23] X. Liu, X. Huang, W. Lin, D. Wang, Y. Diao, H. Li, X. Hui, Y. Wang, A. Xu, D. Wu, D. Ke, New aromatic substituted pyrazoles as selective inhibitors of human adipocyte fatty acid-binding protein, Bioorg. Med. Chem. Lett. 21 (2011) 2949–2952.
[24] H. Cai, Q. Liu, D. Gao, T. Wang, T. Chen, G. Yan, K. Chen, Y. Xu, H. Wang, Y. Li, W. Zhu, Novel fatty acid binding protein 4 (FABP4) inhibitors: virtual screening, synthesis and crystal structure determination, Eur. J. Med. Chem. 90 (2015) 241–250.
[25] F. Lehmann, S. Haile, E. Axen, C. Medina, J. Uppenberg, S. Svensson, T. Lundback, L. Rondahl, T. Barf, Discovery of inhibitors of human adipocyte fatty acid-binding protein, a potential type 2 diabetes target, Bioorg. Med. Chem. Lett. 14 (2004) 4445–4448.
[26] Q. Xu, L. Huang, J. Liu, L. Ma, T. Chen, J. Chen, F. Peng, D. Cao, Z. Yang, N. Qiu, J. Qiu, G. Wang, X. Liang, A. Peng, M. Xiang, Y. Wei, L. Chen, Design, synthesis and biological evaluation of thiazole- and indole-based derivatives for the treatment of type II diabetes, Eur. J. Med. Chem. 52 (2012) 70–81.
[27] Y. Wang, W.K. Law, J.S. Hu, H.Q. Lin, T.M. Ip, D.C. Wan, Discovery of FDA-approved drugs as inhibitors of fatty acid binding protein 4 using molecular docking screening, J. Chem. Inf. Model. 54 (2014) 3046–3050.
[28] Y. Zhou, T. Nie, Y. Zhang, M. Song, K. Li, M. Ding, K. Ding, D. Wu, Y. Xu, The discovery of novel and selective fatty acid binding protein 4 inhibitors by virtual screening and biological evaluation, Bioorg. Med. Chem. 24 (2016) 4310–4317.
[29] G. Floresta, O. Apirakkan, A. Rescifina, V. Abbate, Discovery of high-affinity cannabinoid receptors ligands through a 3D-QSAR ushered by scaffold-hopping

analysis, Molecules 23 (2018) 2183.
[30] G. Floresta, V. Pittala, V. Sorrenti, G. Romeo, L. Salerno, A. Rescifina, Development of new HO-1 inhibitors by a thorough scaffold-hopping analysis, Bioorg Chem 81 (2018) 334–339.
[31] G. Floresta, E. Amata, M. Dichiara, A. Marrazzo, L. Salerno, G. Romeo, O. Prezzavento, V. Pittala, A. Rescifina, Identification of Potentially Potent Heme Oxygenase 1 Inhibitors through 3D-QSAR Coupled to Scaffold-Hopping Analysis, ChemMedChem 13 (2018) 1336–1342.
[32] L. Salerno, E. Amata, G. Romeo, A. Marrazzo, O. Prezzavento, G. Floresta, V. Sorrenti, I. Barbagallo, A. Rescifina, V. Pittala, Potholing of the hydrophobic heme oxygenase-1 western region for the search of potent and selective imidazole-based inhibitors, Eur. J. Med. Chem. 148 (2018) 54–62.
[33] G. Floresta, A. Rescifina, A. Marrazzo, M. Dichiara, V. Pistara, V. Pittala, O. Prezzavento, E. Amata, Hyphenated 3D-QSAR statistical model-scaffold hopping analysis for the identification of potentially potent and selective sigma-2 receptor ligands, Eur. J. Med. Chem. 139 (2017) 884–891.
[34] A. Rescifina, G. Floresta, A. Marrazzo, C. Parenti, O. Prezzavento, G. Nastasi, M. Dichiara, E. Amata, Sigma-2 receptor ligands QSAR model dataset, Data Brief 13 (2017) 514–535.
[35] A. Rescifina, G. Floresta, A. Marrazzo, C. Parenti, O. Prezzavento, G. Nastasi, M. Dichiara, E. Amata, Development of a Sigma-2 Receptor affinity filter through a Monte Carlo based QSAR analysis, Eur. J. Pharm. Sci. 106 (2017) 94–101.
[36] J.M. Luco, F.H. Ferretti, QSAR based on multiple linear regression and PLS methods for the anti-HIV activity of a large group of HEPT derivatives, J. Chem. Inf. Comput. Sci. 37 (1997) 392–401.
[37] A. Surribas, J.M. Amigo, J. Coello, J.L. Montesinos, F. Valero, S. Maspoch, Parallel factor analysis combined with PLS regression applied to the on-line monitoring of Pichia pastoris cultures, Anal. Bioanal. Chem. 385 (2006) 1281–1288.
[38] K. Tuppurainen, S.P. Korhonen, J. Ruuskanen, Performance of multicomponent self-organizing regression (MCSOR) in QSAR, QSPR, and multivariate calibration: comparison with partial least-squares (PLS) and validation with large external data sets, SAR QSAR Environ. Res. 17 (2006) 549–561.
[39] G. Palermo, P. Piraino, H.D. Zucht, Performance of PLS regression coefficients in selecting variables for each response of a multivariate PLS for omics-type data, Adv. Appl. Bioinform. Chem. 2 (2009) 57–70.
[40] T. Asadollahi, S. Dadfarnia, A.M. Shabani, J.B. Ghasemi, M. Sarkhosh, QSAR models for CXCR2 receptor antagonists based on the genetic algorithm for data pre-processing prior to application of the PLS linear regression method and design of the new compounds using in silico virtual screening, Molecules 16 (2011) 1928–1955.
[41] A. Golbraikh, A. Tropsha, Beware of q2!, J. Mol. Graph. Model 20 (2002) 269–276.
[42] T. Cheeseright, M. Mackey, S. Rose, A. Vinter, Molecular field extrema as descriptors of biological activity: definition and validation, J. Chem. Inf. Model 46 (2006) 665–676.
[43] P.H. Olesen, The use of bioisosteric groups in lead optimization, Curr. Opin. Drug Discov. Devel. 4 (2001) 471–478.
[44] A. Burger, Isosterism and bioisosterism in drug design, Prog. Drug. Res. 37 (1991) 287–371.
[45] G.A. Patani, E.J. LaVoie, Bioisosterism: a rational approach in drug design, Chem. Rev. 96 (1996) 3147–3176.
[46] J.J. Irwin, B.K. Shoichet, ZINC–a free database of commercially available compounds for virtual screening, J. Chem. Inf. Model 45 (2005) 177–182.
[47] A.P. Bento, A. Gaulton, A. Hersey, L.J. Bellis, J. Chambers, M. Davies, F.A. Kruger, Y. Light, L. Mak, S. McGlinchey, M. Nowotka, G. Papadatos, R. Santos, J.P. Overington, The ChEMBL bioactivity database: an update, Nucleic Acids Res. 42 (2014) D1083–D1090.
[48] R. Abali, I. Temel Yuksel, M.A. Yuksel, B. Bulut, M. Imamoglu, V. Emirdar, F. Unal, S. Guzel, C. Celik, Implications of circulating irisin and Fabp4 levels in patients with polycystic ovary syndrome, J. Obstet. Gynaecol. (2016) 1–5.
[49] S.A. Abdelwahab, Y. Owada, N. Kitanaka, A. Adida, H. Sakagami, M. Ono, M. Watanabe, F. Spener, H. Kondo, Enhanced expression of adipocyte-type fatty acid binding protein in murine lymphocytes in response to dexamethasone treatment, Mol. Cell Biochem. 299 (2007) 99–107.
[50] S. Bag, S. Ramaiah, A. Anbarasu, fabp4 is central to eight obesity associated genes: a functional gene network-based polymorphic study, J. Theor. Biol. 364 (2015) 344–354.
[51] A.E. Thumser, J.B. Moore, N.J. Plant, Fatty acid binding proteins: tissue-specific functions in health and disease, Curr. Opin. Clin. Nutr. Metab Care 17 (2014) 124–129.
[52] S. Guaita-Esteruelas, J. Guma, L. Masana, J. Borras, The peritumoural adipose tissue microenvironment and cancer. The roles of fatty acid binding protein 4 and fatty acid binding protein 5, Mol. Cell Endocrinol. 462 (2017) 107–118.
[53] K. Kawaguchi, A. Kinameri, S. Suzuki, S. Senga, Y. Ke, H. Fujii, The cancer-promoting gene fatty acid-binding protein 5 (FABP5) is epigenetically regulated during human prostate carcinogenesis, Biochem. J. 473 (2016) 449–461.
[54] S. Guaita-Esteruelas, A. Bosquet, P. Saavedra, J. Guma, J. Girona, E.W. Lam, K. Amillano, J. Borras, L. Masana, Exogenous FABP4 increases breast cancer cell proliferation and activates the expression of fatty acid transport proteins, Mol. Carcinog. 56 (2017) 208–217.
[55] M. Furuhashi, S. Saitoh, K. Shimamoto, T. Miura, Fatty acid-binding protein 4 (FABP4): pathophysiological insights and potent clinical biomarker of metabolic and cardiovascular diseases, Clin. Med. Insights Cardiol. 8 (2014) 23–33.
[56] K. Kawaguchi, S. Senga, C. Kubota, Y. Kawamura, Y. Ke, H. Fujii, High expression of Fatty Acid-Binding Protein 5 promotes cell growth and metastatic potential of colorectal cancer cells, FEBS Open Bio. 6 (2016) 190–199.
[57] T. Yamamoto, M. Furuhashi, T. Sugaya, T. Oikawa, M. Matsumoto, Y. Funahashi, Y. Matsukawa, M. Gotoh, T. Miura, Transcriptome and metabolome analyses in exogenous FABP4- and FABP5-treated adipose-derived stem cells, PLoS One 11 (2016) e0167825.
[58] J. Hao, F. Yan, Y. Zhang, A. Triplett, Y. Zhang, D.A. Schultz, Y. Sun, J. Zeng, K.A.T. Silverstein, Q. Zheng, D.A. Bernlohr, M.P. Cleary, N.K. Egilmez, E. Sauter, S. Liu, J. Suttles, B. Li, Expression of adipocyte/macrophage fatty acid-binding protein in tumor-associated macrophages promotes breast cancer progression, Cancer Res. 78 (2018) 2343–2355.
[59] X. Peng, K. Studholme, M.P. Kanjiya, J. Luk, D. Bogdan, M.W. Elmes, G. Carbonetti, S. Tong, Y.H. Gary Teng, R.C. Rizzo, H. Li, D.G. Deutsch, I. Ojima, M.J. Rebecchi, M. Puopolo, M. Kaczocha, Fatty-acid-binding protein inhibition produces analgesic effects through peripheral and central mechanisms, Mol Pain 13 (2017) 1744806917697007.
[60] G.G. Martin, D. Landrock, S. Chung, L.J. Dangott, D.R. Seeger, E.J. Murphy, M.Y. Golovko, A.B. Kier, F. Schroeder, Fabp1 gene ablation inhibits high-fat diet-induced increase in brain endocannabinoids, J. Neurochem. 140 (2017) 294–306.
[61] H. Huang, A.L. McIntosh, G.G. Martin, D. Landrock, S. Chung, K.K. Landrock, L.J. Dangott, S. Li, A.B. Kier, F. Schroeder, FABP1: a novel hepatic endocannabinoid and cannabinoid binding protein, Biochemistry 55 (2016) 5243–5255.
[62] M.W. Elmes, M. Kaczocha, W.T. Berger, K. Leung, B.P. Ralph, L. Wang, J.M. Sweeney, J.T. Miyauchi, S.E. Tsirka, I. Ojima, D.G. Deutsch, Fatty acid-binding proteins (FABPs) are intracellular carriers for Delta9-tetrahydrocannabinol (THC) and cannabidiol (CBD), J. Biol. Chem. 290 (2015) 8711–8721.
[63] Y.T. Wang, C.H. Liu, H.L. Zhu, Fatty acid binding protein FABP) inhibitors: a patent review (2012–2015), Expert. Opin. Ther. Pat. 26 (2016) 767–776.
[64] Y. Beniyama, K. Matsuno, H. Miyachi, Structure-guided design, synthesis and in vitro evaluation of a series of pyrazole-based fatty acid binding protein (FABP) 3 ligands, Bioorg. Med. Chem. Lett. 23 (2013) 1662–1666.
[65] A. Cheng, S.A. Best, K.M. Merz Jr., C.H. Reynolds, GB/SA water model for the Merck molecular force field (MMFF), J. Mol. Graph Model 18 (2000) 273–282.
[66] J.J. Stewart, Optimization of parameters for semiempirical methods IV: extension of MNDO, AM1, and PM3 to more main group elements, J. Mol. Model 10 (2004) 155–164.
[67] J.J. Stewart, MOPAC: a semiempirical molecular orbital program, J. Comput. Aided Mol. Des. 4 (1990) 1–105.
[68] L. Castanar, G.D. Poggetto, A.A. Colbourne, G.A. Morris, M. Nilsson, The GNAT: a new tool for processing NMR data, Mag. Reson. Chem. 56 (2018) 546–558.